JBC RESEARCH ARTICLE

Glucose-6-phosphate dehydrogenase exerts antistress effects independently of its enzymatic activity

Received for publication, May 15, 2022, and in revised form, October 5, 2022 Published, Papers in Press, October 13, 2022,
https://doi.org/10.1016/j.jbc.2022.102587

Xiaohan Jin[1,‡], **Xuexue Li**[1,‡], **Lifang Li**[2], **Benfu Zhong**[2], **Yang Hong**[2], **Jing Niu**[1,*], **and Binghui Li**[1,3,*]

From the [1]*Department of Biochemistry and Molecular Biology, Capital Medical University, Beijing, China;* [2]*Department of Cancer Cell Biology and National Clinical Research Center for Cancer, Tianjin Medical University Cancer Institute and Hospital, Tianjin, China;* [3]*Beijing Institute of Hepatology, Beijing Youan Hospital, Capital Medical University, Beijing, China*

Edited by Ruma Banerjee

G6PD (glucose-6-phosphate dehydrogenase) is the rate-limiting enzyme in the oxidative pentose phosphate pathway that can generate cytosolic NADPH for biosynthesis and oxidative defense. Since cytosolic NADPH can be compensatively produced by other sources, the enzymatic activity deficiency alleles of G6PD are well tolerated in somatic cells but the effect of null mutations is unclear. Herein, we show that G6PD KO sensitizes cells to the stresses induced by hydrogen peroxide, superoxide, hypoxia, and the inhibition of the electron transport chain. This effect can be completely reversed by the expressions of natural mutants associated with G6PD deficiency, even without dehydrogenase activity, exactly like the WT G6PD. Furthermore, we demonstrate that G6PD can physically interact with AMPK (AMPK-activated protein kinase) to facilitate its activity and directly bind to NAMPT (nicotinamide phosphoribosyltransferase) to promote its activity and maintain the NAD(P)H/NAD(P)$^+$ homeostasis. These functions are necessary to the antistress ability of cells but independent of the dehydrogenase activity of G6PD. In addition, the WT G6PD and naturally inactive mutant also can similarly regulate the metabolism of glucose, glutamine, fatty acid synthesis, and GSH and interact with the involved enzymes. Therefore, our findings reveal the previously unidentified functions of G6PD that can act as the important physiological neutralizer of stresses independently of its enzymatic activity.

The pentose phosphate pathway (PPP) is a metabolic pathway derived from the first product, glucose-6-phosphate (G6P), of glycolysis (1). It generates NADPH for biosynthesis and carbohydrates with different carbons, in particular the pentose, ribose-5-phosphate, for the synthesis of nucleotides. The PPP consists of two distinct phases. G6P is first catalyzed by G6P dehydrogenase (G6PD) to initiate the oxidative phase that produces NADPH and rublose-5-phosphate. In the following nonoxidative phase, 3-, 4-, 5-, 6-, 7-carbon sugars are synthesized, and they can be interconverted to fructose-6-phosphate and glyceraldehyde-3-phosphate that are incorporated into and connected with glycolysis. All the transformations in the second stage are reversible, thus the metabolic intermediates including ribose-5-phosphate can also be initially produced from glycolytic fructose-6-phosphate and glyceraldehyde-3-phosphate, without NADPH being generated. Therefore, the two phases are often designated as the oxidative PPP (oxPPP) and nonoxidative PPP (non-oxPPP).

The reducing power NADPH is mainly utilized for oxidative defense and biosynthesis, in particular, lipogenesis and nucleotides biosynthesis (2, 3). The oxPPP is the major regenerator source of cytosolic NADPH, and its rate-limiting enzyme, G6PD, has been extensively studied (1). Recently, it has been reported that the cytosolic NADPH can also be substantively compensated by NADPH-generating enzymes, such as isocitrate dehydrogenase 1 (IDH1) and malic enzyme 1 (ME1), when G6PD is knocked out in cells (4). It can explain why G6PD deficiency alleles are well tolerated, except that it could bring a risk of acute nonspherocytic hemolytic anemia triggered by exogenous oxidative stressors in red blood cells (5, 6). G6PD deficiency is the commonest disease of human enzyme defect, and its variants are divided into several types based on the report from the World Health Organization (7), class-I G6PD mutants with activity often less than 1% of normal are associated with chronic nonspherocytic hemolytic anemia; class-II has an activity less than 10% of normal; class-III shows 10% to 60% of residual enzyme activity; class-IV are nearly normally active. Intriguingly, up to date, 85 class-I mutants, accounting for about 45% of the total, are identified, but no null mutation has been reported (6, 8). Moreover, the KO of 6-phosphogluconate dehydrogenase (PGD) in the oxPPP, the downstream enzyme of G6PD, even protects cells against oxidative stress (9). These observations suggest that G6PD protein could have other function(s) than the mediation of the oxPPP, which is indispensable to embryonic development. The complete KO of G6PD is indeed reported to be embryonically lethal in mice (10, 11).

Recently, we built up an electron balance model to integrate the metabolic behaviors in the stress conditions and revealed that the oxPPP was shut down and shifted to the non-oxPPP to reduce electron production under hypoxia and the electron transport chain (ETC) inhibition (12). Cells can

‡ Co-first author.
* For correspondence: Binghui Li, bli@ccmu.edu.cn; Jing Niu, niujing@ccmu.edu.cn.

comprehensively reprogram their metabolic pathways to attenuate the stresses by enabling electron transfer (12, 13). Although G6PD KO sensitized cells to the stresses of oxidation, hypoxia, and ETC inhibition (4, 14), we found that the naturally mutated G6PD sufficiently restored the antioxidant activity as the WT enzyme does (14). Here, we demonstrate that G6PD exerts antistress effects depending on its interaction with many proteins instead of its dehydrogenase activity.

Results

The dehydrogenase activity of G6PD is not required for its antistress ability

G6PD is the first and rate-limiting enzyme in the oxPPP that can generate NADPH (Fig. S1*A*), and thus, it was thought to exert a critical antioxidant role. To determine whether the dehydrogenase activity is required for its antioxidant ability, we used CRISPR/cas9–mediated KO system (15) to delete G6PD in HeLa cells and then re-expressed the WT or mutated enzyme. The mutated G6PDs tested here involved natural G6PD deficiency–associated variants including R166H, R257G, 242 to 243Δ with two residues missed, R393H, V394L, N363K, G488V, R198S, and R198P (8), and mechanism-based inactivated mutants, such as proton acceptor His-263 (16) mutated to Ala (H263A), and substrate-binding site Lys-171 mutated to Gln (K171Q), Asp-258 to Ala (D258A) or Lys-360 to Gln (K360Q) (17) (Fig. S2*A*). Our results confirmed that G6PD loss significantly sensitized HeLa cells to hydrogen peroxide (Fig. S2*B*), consistent with recent reports (4, 14). Similar to WT G6PD, all the natural variants completely prevented cells from hydrogen peroxide treatment (Fig. S2*B*). In sharp contrast, mechanism-based mutants almost showed no effect (Fig. S2*B*). Meantime, we measured the dehydrogenase activity of these enzymes using cellular lyses. Most natural mutants showed impaired activities, but R198S and R198P, as well as all the mechanism-based mutants, had no detectable activity (Fig. S2*C*).

Next, we further investigated the functions of G6PD using WT HeLa cells (HeLa/WT), G6PD KO HeLa cells ($HeLa^{KO}$), and KO cells re-expressing Flag-tagged WT G6PD ($HeLa^{WT}$), natural R198P variant ($HeLa^{R198P}$), or mechanism-based H263A mutant ($HeLa^{H263A}$). First, we confirmed again that cellular lyses from $HeLa^{KO}$, $HeLa^{R198P}$, or $HeLa^{H263A}$ did not have G6PD activity, while those from HeLa/WT or $HeLa^{WT}$ cells showed robust activity (Fig. 1*A*). Meanwhile, the product of G6PD, 6-phosphoglucono-σ-lactone (6PGL) (Fig. 1*B*), and the [3-^{2}H]-glucose-labeled NADPH m + 1 generated from oxPPP (18) (Fig. 1*C*) were measured in HeLa/WT or $HeLa^{WT}$ cells but not in $HeLa^{KO}$, $HeLa^{R198P}$, or $HeLa^{H263A}$ cells. The most important product of PPP, ribose 5-phosphate, can be immediately used for *de novo* biosynthesis of IMP, AMP, and GMP (Fig. S1*A*), and their cellular levels did not decline in $HeLa^{KO}$ cells (Fig. S1*B*). We also observed compensatively increased [3-^{2}H]-glucose–labeled NADPH m + 2 in $HeLa^{KO}$, as well as $HeLa^{R198P}$ or $HeLa^{H263A}$ cells (Fig. 1*C*), which resulted from the newly synthesized NADPH incorporating ribose 5-phosphate m + 2 derived from the non-oxPPP (14). These data indicate that the non-oxPPP compensatively supplies the oxPPP-derived intermediates for biosynthesis (Fig. S1*A*).

To further determine the enzymatic activity of these G6PD mutants, we used anti-Flag M2 beads to purify G6PD from $HeLa^{WT}$, $HeLa^{R198P}$, and $HeLa^{H263A}$ cells (Fig. S2*D*) and measured their activities. Our results showed that Flag-G6PD-WT exerted dose- and time-dependent activity, while Flag-R198P and Flag-H263A did not at all (Fig. 1*D*). Next, we purified His-tagged recombinant G6PD proteins expressed in bacteria (Fig. S2*D*) and again demonstrated that G6PD-WT had a robust activity, whereas R198P and H263A mutants were totally inactive (Fig. 1*E*).

In addition to hydrogen peroxide, G6PD-R198P also prevented G6PD-KO HeLa cells from death induced by a superoxide inducer, phenazine methosulfate (PMS) (19), hypoxia, or ETC inhibition with antimycin A, exactly like G6PD-WT (Fig. 1*F*). In fact, even the re-expression of G6PD-H263A also slightly protected $HeLa^{KO}$ cells against hydrogen peroxide, PMS, antimycin A, and hypoxia (Fig. 1*F*). We also observed that $HeLa^{R198P}$ and $HeLa^{WT}$ cells had better colony formation ability and tumor growth in nude mice, compared with $HeLa^{KO}$ cells (Fig. 1, *G* and *H*). Our previous report demonstrated that hypoxia and antimycin A reduced the activity of oxPPP (12). Herein, we found that hydrogen peroxide decreased the [3-^{2}H]-glucose–labeled NADPH m + 1 generated from oxPPP and the total level of cellular NAPDH (Fig. S1*C*), suggesting the suppression of the oxPPP. Therefore, these data, taken together, clearly manifest that the dehydrogenase activity and the oxPPP are not required for the antistress ability of G6PD.

G6PD prevents apoptosis induced by oxidative stress in various cell lines independently of its dehydrogenase activity

We next further tested the sensitivity of HeLa cells expressing G6PD variants to PMS. As shown in Figure 2*A*, $HeLa^{KO}$ and $HeLa^{H263A}$ cells were much more sensitive to PMS treatment, while $HeLa^{WT}$ and $HeLa^{R198P}$ cells displayed similar resistance to PMS, compared with HeLa/WT cells. PMS-induced death in $HeLa^{KO}$ cells was significantly prevented by z-VAD-FMK (an apoptosis inhibitor) (20), but not by necrostatin-1 (a necroptosis inhibitor) (21), or ferrostatin-1 (a ferroptosis inhibitor) (22) (Fig. 2*B*), suggesting the occurrence of caspases-mediated apoptosis. This speculation was further confirmed by results that PMS treatment led to a significant increase in annexin V-staining, cleaved PARP1, and cleaved caspase-3, three indicators of apoptosis, in $HeLa^{KO}$ and $HeLa^{H263A}$ cells but not in $HeLa^{WT}$ and $HeLa^{R198P}$ cells (Fig. 2, *C* and *D*). Next, to expand the generality, we deleted G6PD in MDA-MB-231 and HCT116 cells and re-expressed WT, R198P, or H263A G6PD, respectively. Indeed, G6PD-WT and R198P similarly enabled the G6PD-KO cells resistance to PMS treatments, whereas H263A mutant did not (Fig. 2, *E* and *F*). Therefore, these data suggest that G6PD protects cells against oxidative stress–induced apoptosis independently of its dehydrogenase activity.

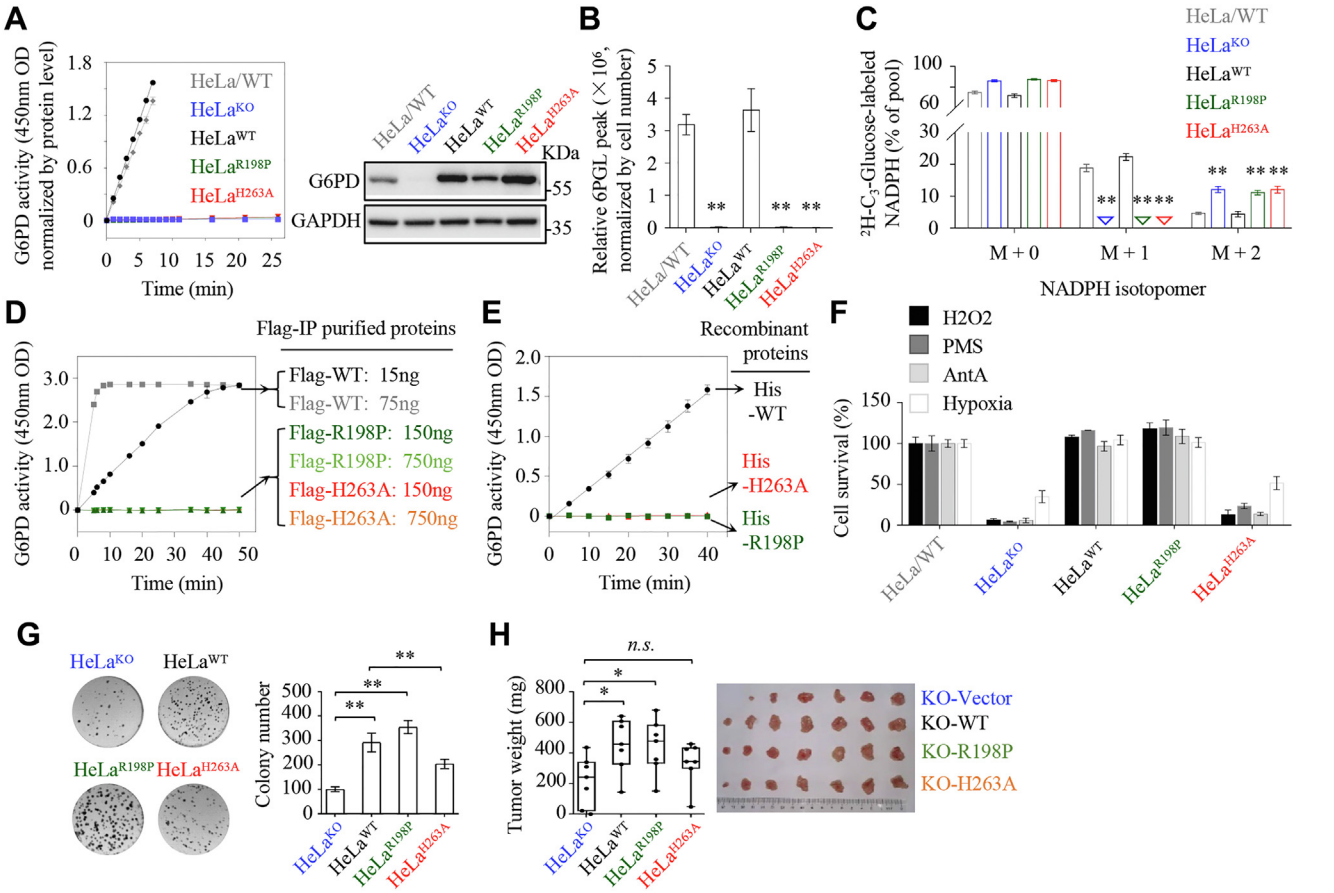

Figure 1. The dehydrogenase activity of G6PD is not required for its antioxidant ability. *A*, enzyme activity of G6PD in HeLa cells lysates with different states of G6PD; Western blotting to verify the expression of G6PD in HeLa/WT cells and the re-expression of the empty vector, G6PD WT, or G6PD mutants (indicated as HeLa^{KO}, HeLa^{WT}, HeLa^{R198P} and HeLa^{H263A}) in G6PD-KO HeLa cells. *B*, the relative abundance of G6PD product 6PGL by LC-MS/MS in HeLa cells with different states of G6PD. *C*, labeling of NADPH's redox active hydrogen in HeLa cells with different states of G6PD. Cells were cultured with the medium containing 10 mM of [3-^{2}H] glucose for 8 h. *D*, enzyme activity of Flag-G6PD-WT, Flag-R198P, or Flag-H263A purified from HeLa^{WT}, HeLa^{R198P}, and HeLa^{H263A} cells. Proteins were verified by Coomassie SDS-PAGE in Fig. S1*D*. *E*, enzyme activity of His-G6PD-WT, His-R198P, or His-H263A purified from *E. coli* expression system. Proteins were verified by Coomassie SDS-PAGE in Fig. S2*D*. *F*, cell survival of HeLa cells with different states of G6PD, as indicated, treated with H_2O_2 (100 μM), PMS(1 μM), and antimycin A (1 μM) for 24 h, and hypoxia (0.5% O_2) for 48 h, normalized to untreated cells. *G*, colony formation by HeLa cells with different states of G6PD. *H*, tumor weight and images of HeLa cells with different states of G6PD in athymic nude mice (n = 7). *$p < 0.05$; **$p < 0.01$ (*t* test); *n.s.*, no significance. In (*B*) and (*C*), asterisk shows comparison with HeLa/WT cells. G6PD, glucose-6-phosphate dehydrogenase; PMS, phenazine methosulfate.

G6PD facilitates AMPK activity independently of its dehydrogenase activity

Recently, it had been reported that G6PD product 6PGL potentially promoted AMPK activation through Src (23). Our recent report also showed that G6PD supported the activation of AMPK pathway (14). Herein, we used 5-amino-4-imidazolecarboxamide ribonucleoside (AICAR) (24) to activate AMPK in HeLa^{WT} and HeLa^{KO} cells and measured the phosphorylation of AMPKα at Thr172 and its specific substrate ACC1 at Ser79. Our results confirmed that the phosphorylations of AMPKα-Thr172 and ACC1-Ser79 in HeLa^{KO} cells were obviously slower than those in HeLa^{WT} cells upon AICAR treatment (Fig. 3*A*). Moreover, pretreatment of AICAR significantly prevented HeLa^{KO} cells from death induced by antimycin A (Fig. 3*B*). To determine whether the dehydrogenase activity of G6PD is required for the activation of AMPK pathway, we used a selective AMPK activator, A-769662, to act on HeLa^{KO}, HeLa^{WT}, HeLa^{R198P}, and HeLa^{H263A} cells and found that it effectively induced the phosphorylation of AMPK-Thr172 and ACC1-Ser79 in HeLa^{WT} and HeLa^{R198P} cells but not in HeLa^{KO} and HeLa^{H263A} cells (Fig. 3*C*). As expected, the pretreatment of HeLa^{KO} cells with A-769662 also prevented antimycin A-induced, PMS-induced, and hydrogen peroxide–induced death (Fig. 3*D*). These results suggest that G6PD exerts antistress roles at least by supporting the activation of AMPK pathway, which does not require its dehydrogenase activity.

Meanwhile, we observed higher basic levels of pAMPK in HeLa^{KO} and HeLa^{H263A} cells than those in HeLa^{WT} and HeLa^{R198P} cells but no apparent difference in the basic levels of pACC1 in these cells (Fig. 3, *A* and *C*). Therefore, G6PD is probably favorable to the activity of AMPK, and its deletion compensatively enhanced the activation of AMPK and the phosphorylations of AMPKα-Thr172. Now, we used an *in vitro* system to test whether G6PD contributed to the activity of AMPK. To simulate the intracellular environment to a greater extent, we expressed Flag-tagged AMPKα1 in HeLa^{KO} cells and the enriched AMPKα1 using anti-Flag M2 beads. The

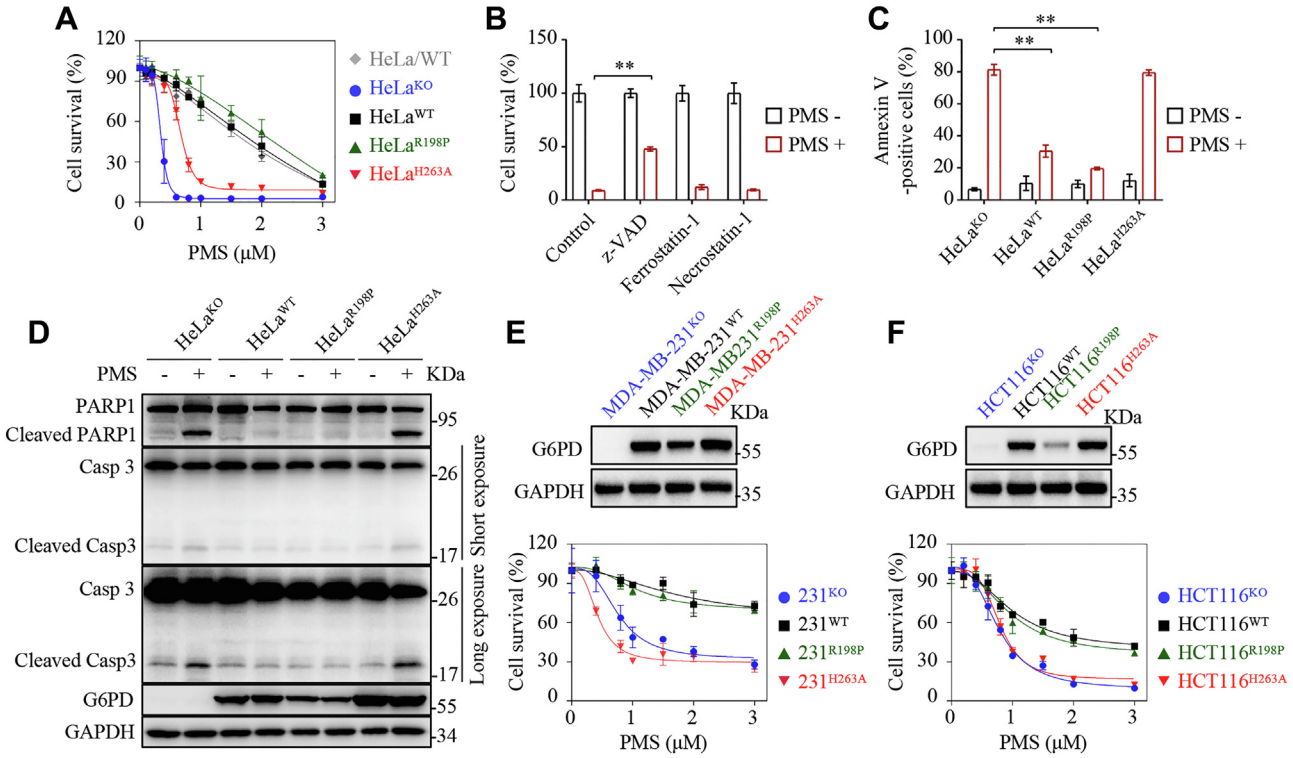

Figure 2. G6PD renders cells resistant to oxidative stress–induced cell apoptosis independently of its dehydrogenase activity. *A*, cell survival of HeLa cells with different states of G6PD treated with different concentrations of PMS for 24 h. *B*, cell survival of HeLa^{KO} cells treated with PMS (1.5 μM) for 24 h after the apoptosis inhibitor Z-VAD (20 μM), the ferroptosis inhibitor ferrostatin-1 (20 μM), and the necroptosis inhibitor necrostatin-1 (10 μM) pretreated for 6 days *C*, flow cytometry analysis for apoptosis in HeLa cells with different states of G6PD treated with or without PMS (1.5 μM) for 24 h. *D*, Western blotting to verify the expression of PARP1, cleaved PARP1, Caspase3, cleaved Caspase3, and G6PD in HeLa^{KO}, HeLa^{WT}, HeLa^{R198P}, and HeLa^{H263A} cells. *E* and *F*, Western blotting to verify the KO of G6PD in MDA-MB-231 cells and HCT116 cells, and the re-expression of the empty vector, G6PD-WT, or G6PD mutants; cell survival of MDA-MB-231 and HCT116 cells with different states of G6PD treated with different concentrations of PMS for 24 h. $^{**}p < 0.01$ (*t* test). G6PD, glucose-6-phosphate dehydrogenase; PMS, phenazine methosulfate.

immunoprecipitates should contain the upstream kinases, so that the addition of ATP to the immunoprecipitates largely increased the level of pAMPKα-Thr172 (Fig. 3*E*). In addition, the immunoprecipitates also contained the downstream substrate ACC1 of AMPK, and we observed that G6PD significantly promoted the phosphorylation of ACC1, indicating the enhanced activity of AMPK by G6PD (Fig. 3*E*). Furthermore, we found that G6PD-R198P also promoted the activity of AMPK, similar to G6PD-WT (Fig. 3*F*).

G6PD directly binds to AMPK independently of its dehydrogenase activity

Next, to determine how G6PD facilitates AMPK activity, we carried out immunoprecipitation (IP) combined with mass spectrometry (MS) to identify different proteins binding to G6PD-WT over to G6PD-H263A (Fig. S3*A*). AMPKγ was found to strongly interact with G6PD-WT (Fig. S3*A* and Table S1). Next, we expressed Flag-tagged G6PD-WT, R198P, and H263A in 293T cells, and our coimmunoprecipitation (Co-IP) results showed that G6PD-WT and R198P mutant obviously precipitated with AMPKα, AMPKβ, and AMPKγ (Fig. 4*A*). By contrast, G6PD-H263A mutant only weakly interacted with AMPK (Fig. 4*A*). We then purified His-tagged G6PD, glutathione-*S*-transferase (GST)–tagged AMPKα1, AMPKβ1, and AMPKγ1 expressed in the bacterial system and demonstrated that G6PD-WT directly interplayed with AMPKα1 (Fig. 4*B*). Purified His-G6PD R198P, but not H263A, also directly interacted with AMPKα1 (Fig. S3*B*). In addition, we also observed the interaction between endogenous AMPKα and G6PD (Fig. 4*C*). Furthermore, we applied Venus-based bimolecular fluorescence complementation to visualize the interaction between proteins using mCherry as the intercontrol (Fig. 4*D*). In order to ensure that these proteins were expressed in equal proportions, we constructed the genes for these proteins in a single ORF, with a self-cleaving P2A peptide inserted between them (Fig. 4*D*). When this plasmid is expressed in cells, the translated protein will be self-cleaved into a Vn (Venus N-terminal 2–173 amino acid residues)-fused protein (P_A), mCherry, and a Vc (Venus C-terminal 155–238 amino acid residues)-fused protein (P_B). If P_A and P_B interacted with each other, Vn and Vc would get close and form a functional Venus to emit yellow fluorescence. We fused Vn to G6PD and Vc to AMPKα1 and observed much stronger yellow fluorescence upon G6PP WT-AMPKα1 and R198P-AMPKα1 interactions than upon H263A-AMPKα1 interaction (Fig. 4*D*). AMPKα consisted of the N-terminal kinase domain and C-terminal regulation domain that was responsible for the binding of AMPKβ and AMPKγ (25) (Fig. 4*E*). Our Co-IP assay showed that G6PD was mainly bound to the kinase domain of AMPKα1 (Fig. 4*E*).

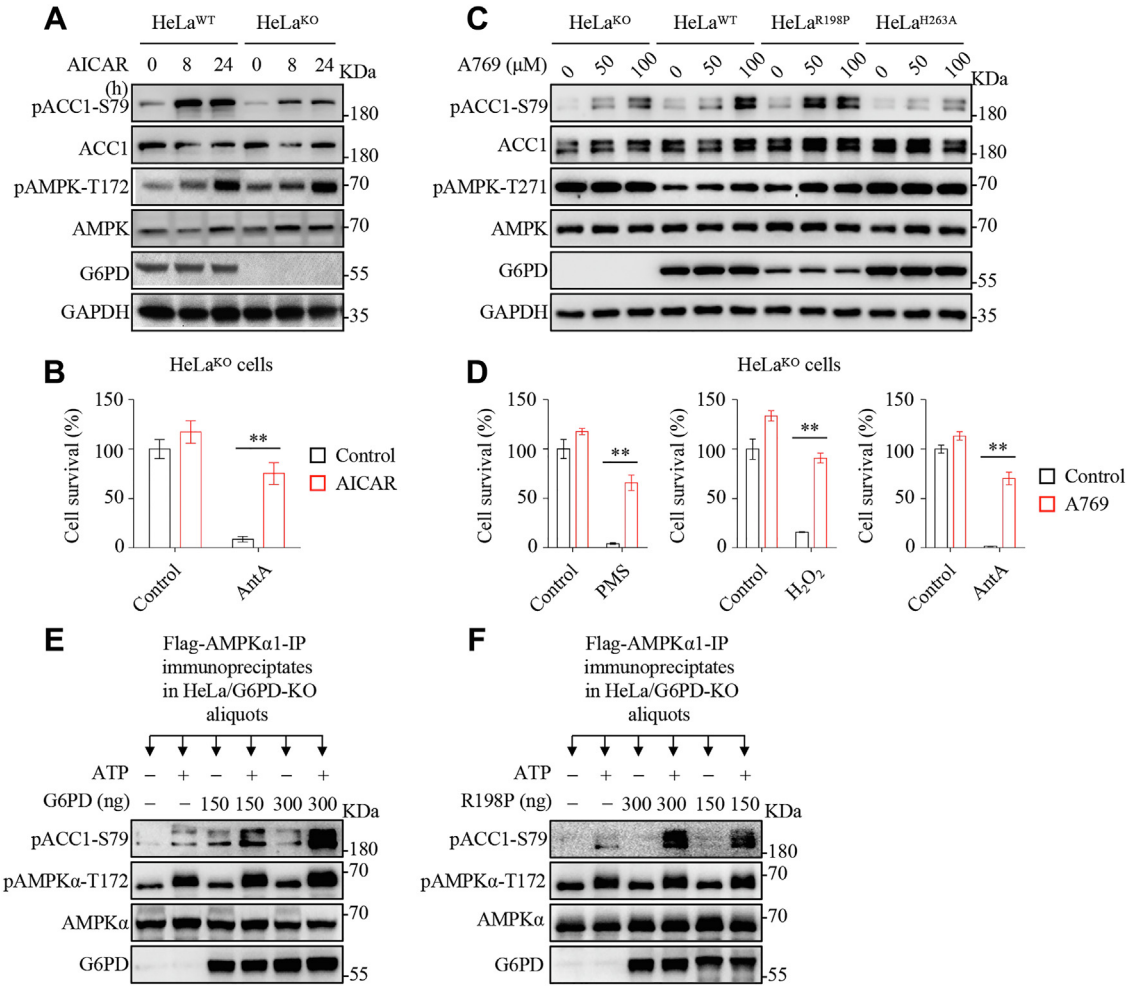

Figure 3. G6PD facilitates AMPK activity independently of its dehydrogenase activity. *A*, Western blotting analysis of G6PD, pACC1-Ser79, ACC1, pAMPKα-Thr172, and AMPK in HeLa/WT and HeLa/G6PD-KO cells treated with 500 μM AICAR for 8 h or 24 h. *B*, cell survival of HeLa/G6PD-KO cells treated with 1 μM antimycin A for 24 h, in the presence or absence of 500 μM AICAR (pretreatment for 12 h). *C*, Western blotting analysis of G6PD, pACC1-Ser79, ACC1, pAMPKα-Thr172, and AMPKα in HeLa cells with different states of G6PD, as indicated, treated with 50 μM or 100 μM A769662 for 8 h. *D*, cell survival of HeLa/G6PD-KO cells treated with or without PMS (1 μM), H_2O_2 (100 μM), antimycin A (1 μM) for 24 h, in the presence or absence of 100 μM A769662 (pretreatment for 16 h). *E* and *F*, Flag-AMPKα1 immunoprecipitates from HeLa/G6PD-KO cells were aliquoted to incubate with recombinant G6PD-Wt or R198P protein in the presence or absence of ATP in an *in vitro* kinase assay. pACC1-Ser79, ACC1, pAMPKα-The172, and AMPKα were detected using Western blot. $^{**}p < 0.01$ (*t* test). AICAR, 5-amino-4-imidazolecarboxamide ribonucleoside; G6PD, glucose-6-phosphate dehydrogenase.

Interestingly, the stress induced by PMS appeared to enhance the interaction between G6PD and AMPK complex (Fig. 4*F*), indicating the involvement of G6PD and AMPK in the stress response. Taken together, these results suggest that G6PD supports AMPK activity probably by physical interaction, regardless of its dehydrogenase activity.

G6PD directly interacts with nicotinamide phosphoribosyltransferase and promote its activity to maintain the homeostasis of NADH/NAD$^+$ and NADPH/NADP$^+$ independently of its dehydrogenase activity

Similar to the previous report (4), NADPH/NADP$^+$ ratio was dramatically reduced in HeLa^{KO} cells, but it was totally reversed by re-expression of G6PD-WT or R198P mutant but not by H263A (Fig. 5*A*). Notably, the cellular NADPH levels kept less changeable in all the cell lines. In contrast, the NADP$^+$ contents were dramatically enhanced in HeLa^{KO} and HeLa^{H263A} cells (Fig. 5*A*). Meanwhile, we measured an increase in the NADH/NAD$^+$ ratio but a decrease in the cellular levels of both NADH and NAD$^+$ in HeLa^{KO} cells and HeLa^{H263A}, compared to HeLa/WT, HeLa^{WT}, and HeLa^{R198P} cells (Fig. 5*B*). These data suggest that G6PD can maintain the NAD(P)H/NAD(P)$^+$ homeostasis, and this effect does not depend on its dehydrogenase activity.

The biosynthesis of NAD$^+$ and NADP$^+$ is accomplished through either *de novo* pathway from tryptophan or the salvage pathway from nicotinamide, nicotinic acid, or nicotinic acid riboside (Fig. S4*A*). We detected the expressions of the involved enzymes and found no phenotype-associated difference between HeLa^{KO}, HeLa^{WT}, and HeLa^{R198P} cells (Fig. S4*B*). We then used [2,4,5,6-^{2}H]-nicotinamide to trace the biosynthesis of NAD$^+$ and NADP$^+$ (Fig. 5*C*) (26), and our results showed that the fraction of newly synthesized NAD$^+$ m + 3 significantly decreased in HeLa^{KO} cells, which was reversed by re-expression of G6PD-WT and R198P mutant (Fig. 5*D*). In

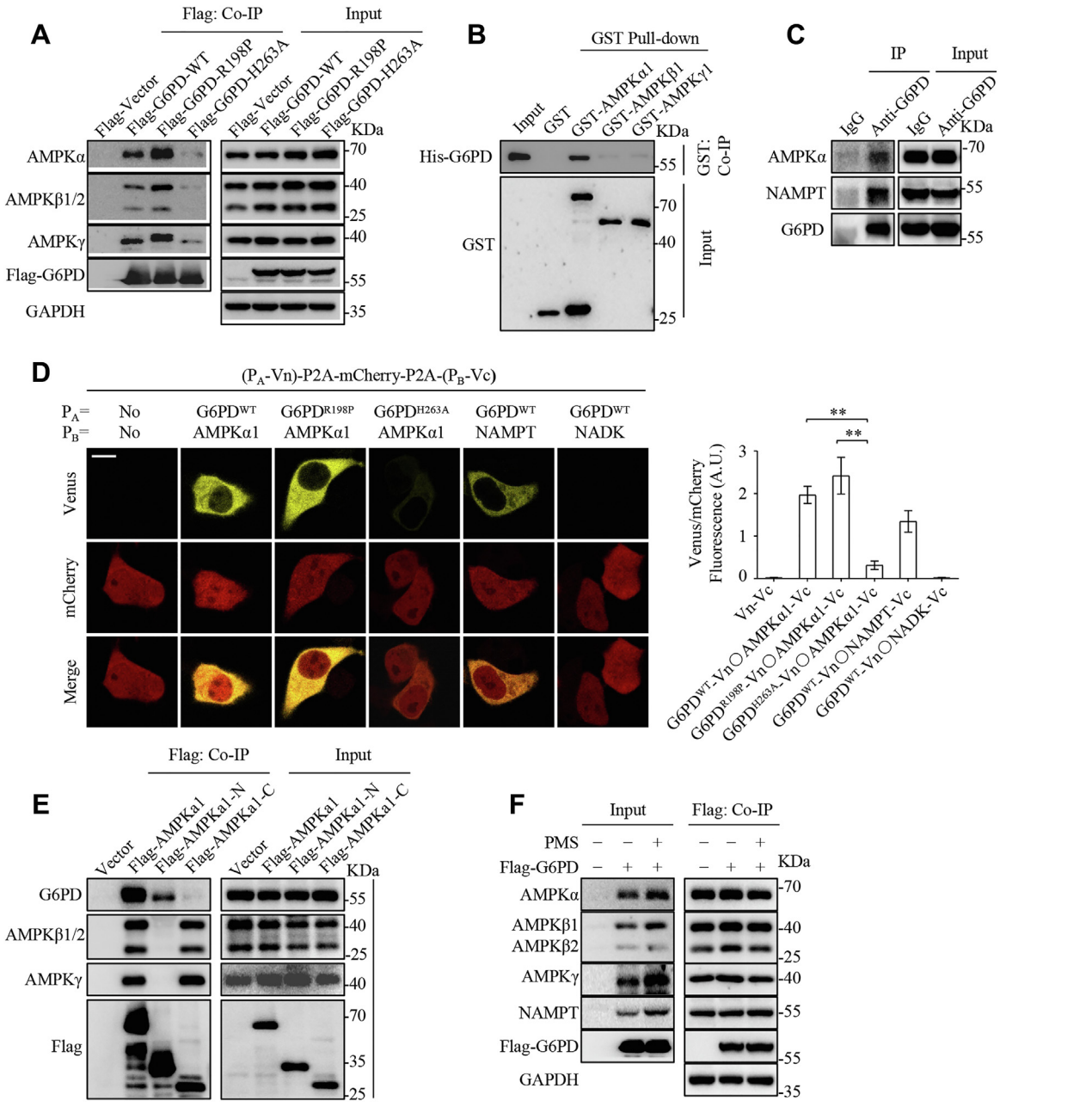

Figure 4. G6PD directly binds to AMPK independently of its dehydrogenase activity. *A*, HEK293T cells were transfected with vector, Flag-G6PD-WT, Flag-G6PD-R198P, or Flag-G6PD-H263A plasmid and then co-IP assays were performed 48 h after transfection using anti-FLAG affinity M2 beads, followed by Western blot. *B*, interaction of GST-AMPKα1, GST-AMPKβ1, or GST-AMPKγ1 with His-G6PD in the reaction mixtures was analyzed by a GST-pulldown assay. *C*, the interaction between endogenous G6PD and AMPKα or NAMPT was determined in HeLa cells. *D*, validation of the interaction between AMPKα, NAMPT, NADK1, and G6PD by bimolecular fluorescence complementation (BiFC) analysis. The scale bar represents 10 μm. Randomly selected representative cells were quantified for fluorescence intensity ratios of vennus/mCherry (n = 6). *E*, HEK293T cells were transfected with vector, Flag-AMPKα1, Flag-AMPKα1-N, or Flag-AMPKα1-C plasmid and then co-IP assays were performed 48 h after transfection using anti-FLAG affinity M2 beads, followed by Western blot. *F*, HEK293T cells were transfected with vector, Flag-G6PD-WT plasmid, and then treated with or without PMS (1 μM) for 8 h. Co-IP assays were performed using anti-FLAG affinity M2 beads followed by Western blot. $^{**}p < 0.01$ (*t* test). Co-IP, coimmunoprecipitation; G6PD, glucose-6-phosphate dehydrogenase; NAMPT, nicotinamide phosphoribosyltransferase; PMS, phenazine methosulfate.

contrast, the labeled fractions of $NADP^+$ were similar in HeLa/WT, $HeLa^{WT}$, $HeLa^{R198P}$, $HeLa^{KO}$, and $HeLa^{H263A}$ cells (Fig. 5*D*). These results suggest that G6PD KO could suppress NAD^+ biosynthesis while promoting $NADP^+$ biosynthesis.

Recently, it has been reported that G6PD promotes $NADP^+$ biosynthesis by directly binding to NADK to activate its activity (27). However, we expressed Flag-G6PD in 293T cells and the Co-IP assay did not detect the interaction between G6PD and NADK (Fig. S4*C*). Furthermore, we purified G6PD and NADK and still did not observe the interaction between them in the *in vitro* pull-down assay (Fig. S4*D*). Moreover, we found that G6PD did not significantly affect the activity of NADK (Fig. S4*E*). Therefore, we further detected the interaction of G6PD with nicotinamide phosphoribosyltransferase

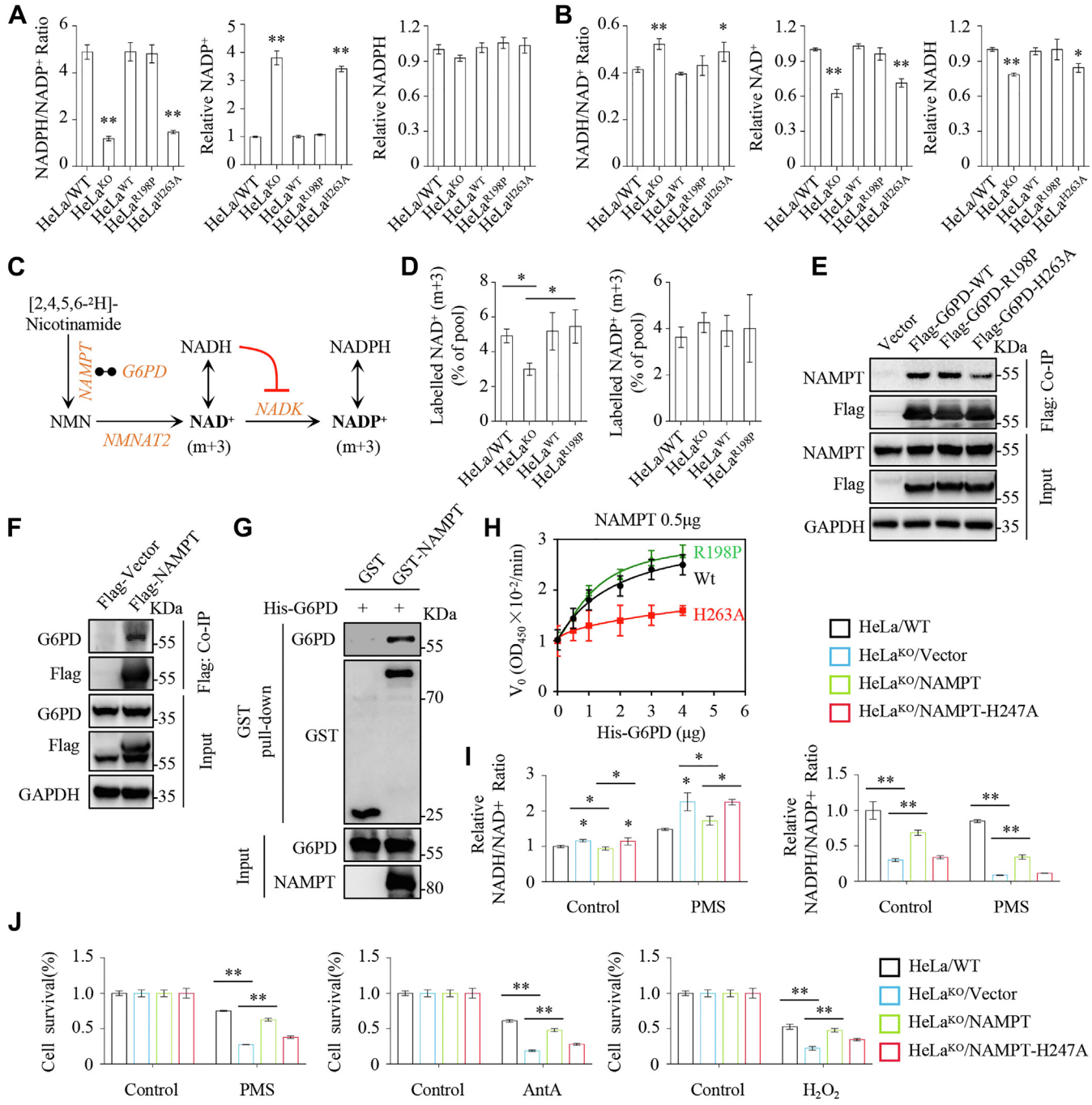

Figure 5. G6PD interacts with NAMPT to promote its activity and maintain NAD(P)H/NAD(P)$^+$ homeostasis independently of its dehydrogenase activity. *A*, NADPH/NADP$^+$ ratio and NADP$^+$ or NADPH relative levels were determined in HeLa cells with different states of G6PD. *B*, NADH/NAD$^+$ ratio and NAD$^+$ or NADH relative levels were assayed in HeLa cells with different states of G6PD. *C*, schematic representation of isotopic tracing for *in vivo* NAMPT function. *D*, mass isotopomer analysis of NAD$^+$ and NADP$^+$ in HeLa cells with different states of G6PD cultured with the medium containing 32.8 μM of [2,4,5,6–2 H]-nicotinamide for 1 h. *E*, HEK293T cells were transfected with vector, Flag-G6PD-WT, Flag-G6PD-R198P, or Flag-G6PD-H263A plasmid and then co-IP assays were performed 48 h after transfection using anti-FLAG affinity M2 beads, followed by Western blot. *F*, HEK293T cells were transfected with vector, Flag-NAMPT plasmid, and then co-IP assays were performed 48 h after transfection using anti-FLAG affinity M2 beads followed by Western blot. *G*, interaction of GST-NAMPT with His-G6PD in the reaction mixtures was analyzed by a GST pull-down assay. *H*, velocity of NAMPT enzymatic reaction in the presence of 0.5 μg of GST-NAMPT and different amounts of His-G6PD-WT, His-R198P, or His-H263A purified from *E. coli* expression system. Proteins were verified by Coomassie SDS-PAGE in Fig. S5*B*. *I*, NADH/NAD$^+$ and NADPH/NADP$^+$ ratios of HeLa/WT and HeLa/G6PD-KO cells expressing vector, NAMPT, or NAMPT^{H247A} cells. *J*, cell survival of HeLa/WT and HeLa/G6PD-KO cells expressing vector, NAMPT, or NAMPT^{H247A} cells, as indicated, treated with PMS (1 μM), antimycin A (1 μM) or H_2O_2 (100 μM) for 24 h, normalized to untreated cells. *$p < 0.05$; **$p < 0.01$ (*t* test). Co-IP, coimmunoprecipitation; G6PD, glucose-6-phosphate dehydrogenase; NAMPT, nicotinamide phosphoribosyltransferase; PMS, phenazine methosulfate.

(NAMPT) and NMNAT2, the two enzymes involved in NAD$^+$ biosynthesis, and found that G6PD did not physically bind to NMNAT2 (Fig. S4*F*) but coimmunoprecipitated with NAMPT (Fig. 5*E*). Moreover, G6PD-WT and R198P mutant showed much stronger binding to NAMPT than H263A (Fig. 5*E*). In reverse, NAMPT also coprecipitated with G6PD (Fig. 5*F*). We

then purified the recombinant GST-NAMPT and His-G6PD and demonstrated the direct interaction between them (Fig. 5*G*). The Co-IP results also detected the interaction between the endogenous G6PD and NAMPT (Fig. 4*C*). The bimolecular fluorescence complementation assay further confirmed that G6PD interacted with NAMPT but not NADK (Fig. 4*D*). Taken together, these data emphasize that G6PD bind to NAMPT. Therefore, we next investigated whether G6PD affected the activity of NAMPT using an *in vitro* assay. Our results showed that G6PD-WT and R198P mutant accelerated the activity of NAMPT in a dose-dependent manner (Figs. 5*H* and S5, *A* and *B*). By contrast, H263A mutant only slightly activated NAMPT (Figs. 5*H* and S5*A*). Now we overexpressed Flag-tagged WT NAMPT and inactivated NAMPT-H247A mutant in HeLa^{KO} cells (Fig. S5*C*). We observed that Flag-NAMPT, not Flag-NAMPT-H247A, significantly restored the cellular levels of NAD^+, NADH, $NADP^+$, and NADPH (Fig. S5, *D* and *E*) and maintained the homeostasis of NADH/NAD^+ and NADPH/$NADP^+$, under the normal condition or treatment with PMS (Fig. 5*I*). NAD^+ is the substrate of NADK but NADH potently inhibited NADK (Fig. S5*F*). Therefore, the ratio of NADH/NAD^+ should tightly control the biosynthesis of $NADP^+$.

In addition, the forced expression of Flag-NAMP significantly protected HeLa^{KO} cells against the treatments with PMS, antimycin A, or hydrogen peroxide (Fig. 5*J*). These results suggest that G6PD maintains the homeostasis of NADH/NAD^+ and NADPH/$NADP^+$ independently of its dehydrogenase activity, at least partially through promoting NAMPT activity.

G6PD regulates the metabolism of glucose, GSH, glutamine, and fatty acids independently of its dehydrogenase activity

Although the aforementioned results demonstrated that G6PD supported AMPK activation and promoted NAMPT activity, blocking AMPK by compound C and/or NAMPT by FK886 in HeLa cells did not mimic the sensitivity of HeLa^{KO} cells to PMS (Fig. S5*G*). It suggests that G6PD neutralizes stresses most like through many pathways. Among the proteins preferentially interacting with G6PD-WT over H263A mutant (Table S1), PFKP, GAPDH, and ACLY were also identified. We then expressed Flag-G6PD variants in 293T cells and confirmed that G6PD-WT and R198P mutant bound to PFKP, GAPDH, and ACLY much stronger than H263A mutant (Fig. 6*A*). PFKP and GAPDH were involved in glycolysis and glycerol production (Fig. 6*B*). We observed that G6PD-KO promoted glucose uptake and lactate excretion in HeLa cells, which was restored by re-expression of G6PD-WT or R198P mutant (Fig. 6, *C* and *D*). Like lactate, glycerol excretion is also associated with stresses (12). We indeed detected an increased excretion of glycerol in HeLa^{KO} and HeLa^{H263A} cells but not in HeLa/WT, HeLa^{WT}, and HeLa^{R198P} cells (Fig. 6*E*). Meanwhile, we also observed the corresponding interaction between G6PD-WT or R198P mutant, not H263A, and PGP (Fig. 6*A*), a critical enzyme responsible for glycerol production (Fig. 6*B*). GAPDH was an important regulator to determine whether glucose was metabolized to lactate or glycerol. Therefore, we measured the activity of GAPDH in cell lysis and found that cellular GAPDH activities in HeLa^{KO} and HeLa^{H263A} cells were reduced (Fig. 6*F*). Furthermore, we added purified G6PD-WT, R198P, and H263A to the purified GADPH reaction buffer and confirmed that G6PD-WT and R198P potently activated GAPDH (Fig. 6*G*). These data suggest that G6PD can regulate glucose metabolism independently of its dehydrogenase activity.

ACLY is involved in *de novo* fatty acid synthesis. We previously reported that G6PD-KO suppressed glutamine-initiated fatty acid synthesis through the reductive pathway (14). Here, we confirmed that the fraction of $^{13}C_5$-glutamine-labeled palmitate was reduced in HeLa^{KO} and HeLa^{H263A} cells but restored in HeLa/WT, HeLa^{WT}, and HeLa^{R198P} cells (Fig. 6*H*). IDH1 is a critical enzyme for the reductive metabolism of glutamine, and we also detected an interaction between IDH1 and G6PD-WT or R198P mutant (Fig. 6*A*). Taken together, G6PD promotes glutamine-initiated fatty acids independently of its dehydrogenase activity, possibly depending on its interaction with enzymes in this pathway, which plays a critical role against some stresses.

GSH and GSSG are the principal components of the antioxidant defense system. The levels of total GSH (GSH + GSSG) and the ratios of GSH/GSSG in HeLa/WT, HeLa^{WT}, HeLa^{R198P}, HeLa^{KO}, and HeLa^{H263A} cells showed no significant difference in the normal condition (Fig. 6*I*). However, the total GSH content and GSH/GSSG ratio significantly decreased in HeLa^{KO} cells treated with PMS, which was totally reversed by the expression of G6PD-WT and R198P mutant but not H263A, compared with HeLa/WT (Fig. 6*I*). These data suggest that G6PD contributes to GSH biosynthesis independently of its dehydrogenase activity. Meanwhile, G6PD-WT and R198P mutant, not H263A, were strongly bound to GCLC and GCLM, the two subunits of glutamate cysteine ligase and GSH synthetase (GSS), involved in GSH biosynthesis (Fig. 6, *A* and *B*). In addition, our Co-IP assay results also showed that G6PD-WT and R198P mutant interacted with GSH reductase (GSR), a critical enzyme required for the GSH system. These results suggest that G6PD exerts an important role in supporting the GSH system to neutralize oxidative stress, which is independent of its dehydrogenase activity while associated with its interaction with the enzymes. Our data also further demonstrated that supplementation with GSH or its permeable precursor, N-acetylcysteine (NAC), significantly prevented HeLa^{KO} cells from death induced by PMS and antimycin A (Fig. 6*J*).

Discussion

It has long been established that G6PD-mediated oxPPP generates NADPH for cells to support anabolism, especially *de novo* synthesis of fatty acids, and attenuate oxidative stress. Our previous study has shown that G6PD KO does not affect glucose-derived fatty acid biosynthesis but suppresses glutamine-initiated lipogenesis *via* the reductive pathway (14). G6PD KO cells are much more sensitive to the stresses, such

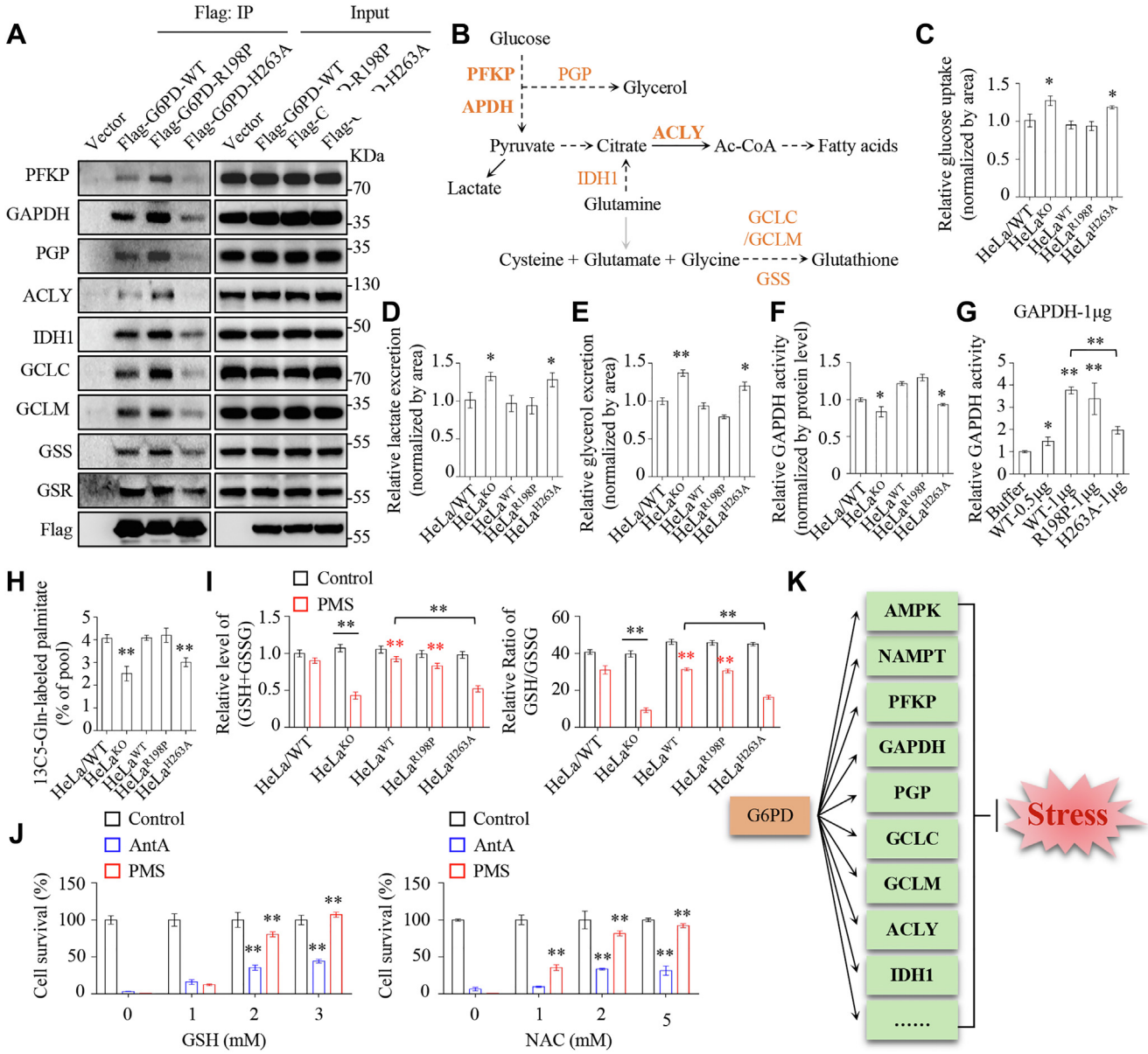

Figure 6. G6PD regulates cellular metabolism independently of its dehydrogenase activity. *A*, HEK293T cells were transfected with vector, Flag-G6PD-WT, Flag-G6PD-R198P, or Flag-G6PD-H263A plasmid and then co-IP assays were performed 48 h after transfection using anti-FLAG affinity M2 beads, followed by Western blot. *B*, schematic diagram of the metabolism of glucose, GSH, glutamine, and fatty acids. *C–E*, glucose uptake (*C*), lactate excretion (*D*), and glycerol excretion (*E*) in HeLa cells with different states of G6PD, as indicated, under the normal condition. *F*, enzyme activity of GAPDH in HeLa cells lysates with different states of G6PD. *G* and *H*, relative labeled carbons in fatty acids in HeLa cells with different states of G6PD cultured with $^{13}C_5$-glutamine for 48 h in the normal condition. *I*, the total GSH (GSH + GSSG) and the ratio of GSH/GSSG was determined in HeLa cells with different states of G6PD treated with or without PMS (1 μM) for 6 h. *J*, cell survival of HeLa^{KO} cells treated with antimycin A (1 μM) or PMS (1 μM) for 24 h in the presence of different concentrations of GSH and NAC (pretreatment for 6 h). *K*, the working model of antistress roles of G6PD by binding to AMPK, NAMPT, PFKP, GAPDH, PGP, GCLC, GCLM, ACLY, IDH1, and other proteins. *$p < 0.05$; **$p < 0.01$ (*t* test). G6PD, glucose-6-phosphate dehydrogenase; NAMPT, nicotinamide phosphoribosyltransferase; PMS, phenazine methosulfate.

as hydrogen peroxide, superoxide, ETC inhibition, and hypoxia. However, the naturally G6PD mutants, especially the inactive R198P variant, can completely wipe off all the abnormal phenotypes, indicating that the dehydrogenase activity of G6PD and its activity-driven NADPH generation in the oxPPP are not required for these biological actions. Instead, our findings reveal that G6PD can facilitate AMPK activity and activate NAMPT activity to maintain the homeostasis of NAD(P)H/NAD(P)$^+$, and may also regulate many other proteins/pathways, through physical interactions, which could integrally protect cells against stresses (Fig. 6*K*).

Why is the dehydrogenase activity of G6PD considered indispensable for its physiological functions? The most intuitive reason for this may be G6PD deficiency. The red blood cells rely on G6PD enzymatic activity and the downstream oxPPP (5), most likely because they lack the complicated metabolism that could not provide substitutive NADPH and not be rewired to adapt to the stresses. However, in somatic

cells, NADPH can be readily compensated by other sources, such as IDH1 and ME1, for the lack of the oxPPP resulting from G6PD KO in cells, as revealed in previous reports (4, 14). Therefore, cells can accommodate the mutations in G6PD that impair its dehydrogenase activity, which leads to G6PD deficiency. Fortunately, these naturally mutated G6PDs, functionally selected through embryonic development, still keep the necessary ability to resist the stresses independently of their dehydrogenase activity. However, in most, if not all, studies on G6PD, mechanism-based mutants are used as the negative controls. These mechanism-based mutants, such as H263A, K171Q, D258A, and K360Q used in the current study, do not render cells resistant to stresses, which leads to a widely accepted conclusion that the dehydrogenase activity of G6PD is necessary for its antistress functions. Herein, we compare natural R198P variant and mechanism-based H263A mutant, both are enzymatically dead, with WT G6PD and find that they show differential interactions with some proteins associated with the functions of G6PD. This may be attributed to their conformational alterations. However, we cannot rule out the possibility that natural G6PD mutants have other enzymatic activities requiring active sites of dehydrogenase. The detailed underlying mechanisms remain to be further explored, but our current data clearly demonstrate that G6PD can antagonize stresses, regardless of its enzymatic activity, which is complementary to its typical action mediating the oxPPP. Taken together, our findings help us to better understand the physiological roles of G6PD and its association with human diseases.

Experimental procedures

General reagents

A769662 was obtained from Selleck. AICAR, compound C, FK866, Z-VAD, ferrostatin-1, and necrostatin-1 were obtained from MedChemExpress. [3-^{2}H]-glucose, $^{13}C_5$-glutamine, and [2,4,5,6-^{2}H]-nicotinamide were purchased from Cambridge Isotope Laboratories. PMS, antimycin A, and all general chemicals were obtained from Sigma unless otherwise described.

Cell culture

HeLa, MDA-MB-231, HCT116, and HEK-293T cells were obtained from ATCC. All the cells were cultured in high glucose Dulbecco's modified Eagle's medium (DMEM) supplemented with 10% fetal bovine serum (FBS) (BioInd) and 50 IU penicillin/streptomycin (Invitrogen) in a humidified atmosphere with 5% CO_2 at 37 °C. Hypoxia studies were carried out at 0.5% oxygen.

Plasmids and lentivirus production

The DNA fragments corresponding to the full-length of WT and mutated G6PDs, NAMPT, and mutated NAMPT were amplified by PCR and cloned into pCDH-Neo-CMV or pCDH-puro-CMV vectors (Clontech) for stably expression in cells. All plasmids were verified by sequencing (Genewiz). Viral packaging was done according to a previously described protocol (28). Briefly, expression plasmids, pCMV-dR8.91 and pCMV-VSV-G, were cotransfected into 293T cells at a final concentration of 10 μM PEI, then media containing virus was collected 48 h after transfection, filtered with a PES filter (0.22 μm, Millipore), and stored at −80 °C. Cancer cells were infected with the viruses at the titer of 100% infection in the presence of polybrene (10 μg/ml) for 12 to 24 h and then cells were selected with puromycin or neomycin.

CRISPR KO of G6PD

G6PD was deleted from HeLa, MDA-MB-231, and HCT116 cells using the CRISPR–Cas9 system. pCDH-Cas9-2A-GFP-BSD was used to express Cas9. Single-guide RNAs were cloned into pLentiGuide-puro-vector (15) linearized with BsmBI. The following are the target sequences for G6PD: GATCCGCGTGCAGCCCAACG. Cells were cotransfected with the plasmids expressing single-guide RNA and Cas9-EGFP and then were cultured for 48 h. Single cells were seeded in a well of 96-well plate by fluorescence activating cell sorter based on green fluorescence and allowed to grow until colonies formed. Clones were grown in DMEM containing 20% FBS. Functional gene deletion was confirmed by targeted genomic sequencing followed by Western blotting.

Immunoblotting

For protein extracts, cells were lysed in ice-cold radioimmunoprecipitation assay lysis buffer containing a protease inhibitor cocktail (Roche). Lysates were cleared by 15 min centrifugation at 13,000*g* at 4 °C and protein concentrations were determined with bicinchoninic acid assay kit (Thermo Fisher Scientific). Normalized protein lysates were subjected to SDS-PAGE, followed by transferring to polyvinylidene difluoride filters (Millipore) and immunoblotting with the indicated antibodies. Anti-G6PD (catalog no.: #25413-1-AP), GAPDH (catalog no.: #60004-1-lg), ACC1 (catalog no.: #21923-1-AP), GST(catalog no.: #10000-0-AP), c-*myc* (catalog no.: #10828-1-AP), NAMPT (catalog no.: #11776-1-AP), NADK (catalog no.: #15548-1-AP), PFKP (catalog no.: #13389-1-AP), GCLC (catalog no.: #12601-1-AP), GCLM (catalog no.: #14241-1-AP), ACLY (catalog no.: #15421-1-AP), NAPRT1 (catalog no.: #13549-1-AP), QPRT (catalog no.: #25174-1-AP), GSS (catalog no.: #67598-1-lg), GSR(catalog no.: #18257-1-AP), Caspase 3/p17/p19 (catalog no.: #19677-1-AP), and PARP1(catalog no.: #13371-1-AP) were obtained from ProteinTech Inc Anti-AMPKα (catalog no.: #5831), pAMPKα (catalog no.: #2535), AMPKβ1/2 (catalog no.: #4150), AMPKγ (catalog no.: #4187), and pACC1 (catalog no.: #3661) were obtained from Cell Signaling Technology. Anti-NMNAT1 (catalog no.: #ab45652), NMNAT2 (catalog no.: #ab56980), and NADSYN1 (catalog no.: #ab171942) were obtained from Abcam. Anti-FLAG (catalog no.: #MBL-3L) was obtained from MBL Bio. Anti-ITGB1BP3 (catalog no.: #PA5-113755) was obtained from Thermo Fisher Scientific. Anti-PGP (catalog no.: #sc-390883) was obtained from Santa Cruz. The goat anti-rabbit IgG/horseradish peroxidase (catalog no.: #ZDR-5306) and the goat anti-mouse IgG/horseradish peroxidase (catalog

no.: #ZDR-5307) secondary antibodies were obtained from ZSGB-Bio. The blotted filters were visualized for signals using enhanced chemiluminescence reagents (GE Healthcare) according to the manufacturer's instructions.

Cell survival assay

Cells were triplicately plated onto 12-well dishes, with an initial seeding density of 1.5×10^5 cells per well for HeLa, MDA-MB-231, and 3.0×10^5 cells for HCT116. After overnight or 24 h incubation for cells to adhere, three wells were counted as the initial number at the time of treatment. Then, cells were washed twice in PBS and 1 ml of media containing treatment was added. Cells were treated with H_2O_2 (100 μM), PMS (1 μM), antimycin A (1 μM), compound C (5 μM), and FK866 (1 μM) for 24 h. Hypoxia studies were carried out at 0.5% oxygen for 24 h. To detect the rescue effect of G6PD KO cells under the stimulations with PMS, H_2O_2, or antimycin A, cells were pretreated with 100 μM A769662 for 16 h, 500 μM AICAR for 12 h, 1 mM GSH, or 1 mM NAC for 6 h.

Colony formation assay

Cells were cultured in 12-well plates (500 cells per well) for 14 to 21 days based on the experiment. Colonies were fixed with methanol and stained with 0.1% crystal violet in 20% methanol for 15 min. Analysis was performed on the basis of integrated density using NIH ImageJ Software. All experiments were performed in triplicate.

Apoptosis assay

For apoptosis analysis, a PE Annexin V Apoptosis Detection Kit I (BD-559763) was used. Twenty-four hours after PMS (1.5 μM) stimulation, the medium was changed to a new medium containing 5 μl of Annexin V-PE and 5 μl of 7AAD for 15 min at room temperature (RT) in dark, according to the manufacturer's protocol. Then, the cellular apoptosis was analyzed by using a Gallios Flow Cytometer (Beckman Coulter).

Measurements of NAD^+, NADH, $NADP^+$, and NADPH using a bioluminescent enzyme-based assay

NAD^+, NADH, $NADP^+$, and NADPH were measured using the NAD/NADH-Glo Assay and NADP/NADPH-Glo Assay (catalog no.:#G9072/G9082 from Promega), according to the manual instructions with modifications. Briefly, 1.5 × 10^5 cells per well were seeded in 12-well plates overnight or 24 h and then incubated with the treatment medium for the desired period. Cells were quickly washed once with PBS and then extracted with 400 μl ice-cold lysis buffer. To measure NADH or NADPH, 150 μl of the samples were moved to wells of a 48-well plate and incubated at 60 °C for 15 min. To measure NAD^+ or $NADP^+$, another 150 μl of the samples were moved to wells of another 48-well plate containing 75 μl of 0.4 N HCl and incubated at 60 °C for 15 min. Samples were equilibrated to RT and then each was quenched by neutralizing with 150 μl of HCl/Trizma solution (for NADH or NADPH measurement) or 75 μl of 0.5 M Tris-base (for NAD^+ or $NADP^+$ measurement). Twenty microliters of the neutralized samples were moved to wells of a 384-well solid black luminometer plate (catalog no.:#3570 from Corning) and mixed with 20 μl of the newly prepared NAD/NADH-Glo or NADP/NADPH-Glo detection reagent. The mixtures were gently shaken for 50 min at RT and then the luminescence was measured using a Synergy H1 Hybrid Multi-Mode reader (BioTek). To acquire the relative abundance of NAD^+, NADH, $NADP^+$, and NADPH in cell lysis, the measured signals were normalized by cell number from the parallel experiments.

IP and MS

For IP of FLAG-tagged proteins, cells were harvested using IP lysis buffer (50 mM Tris–HCl at pH 8.0, 150 mM NaCl, 1% NP-40, and 1 mM EDTA). Lysates were rocked for 1 h and centrifuged at 13,000*g* at 4 °C for 15 min. Supernatants were incubated with 30 μl of 50% slurry of anti-FLAG M2 Affinity Gel at 4 °C for 4 h. Gel was sequentially washed with lysis buffers three times. Recombinant proteins were eluted using 30 μl of 400 μg/ml peptide at 4 °C for 2 h and centrifuged at 5000*g* at 4 °C for 5 min. The eluates were collected and resolved on NuPAGE 4% to 12% Bis–Tris gel (Invitrogen), silver-stained using Pierce silver stain kit, and bands 1 to 4, as shown in Fig. S3*A*, were prepared and subjected to LC-MS/MS (Agilent 6340) detection.

Protein purification

His-G6PD-WT, His-R198P, and His-H263A expressed from the pET-28a vector were purified from *Escherichia coli* BL21 after induction with 1 mM IPTG for 20 h at 18 °C. GST-NAMPT, GST-NADK, GST-AMPKα1, GST-AMPKβ1, and GST-AMPKγ1 expressed from the pGEX-6P-1 vector were purified from *E. coli* BL21 too. Single colonies were first verified for similar expressions and then selected clones were used for purifications. Bacterial pellets were resuspended in ice-cold resuspension buffer and sonicated for completely lysed. Lysates were clarified by centrifuged at 16,000*g* for 20 min at 4 °C and supernatants were collected for subsequent purification. Recombinant GST-fusion proteins were purified using GSH-Sepharose 4B (GE Healthcare). His-tagged proteins were purified using a Ni^{2+}-Sepharose affinity column (GE Healthcare). For Flag-G6PD-WT, Flag-R198P, and Flag-H263A protein purification from $HeLa^{WT}$, $HeLa^{R198P}$, and $HeLa^{H263A}$ cells, cells were harvested using IP lysis buffer. The specific steps of protein purification are the same as the aforementioned protocol of immunoprecipitation. All purified proteins were quantified on a Coomassie-stained gel with adjacent bovine serum albumin standards. GAPDH was commercially obtained from Abcam (catalog no.: #ab204732).

GST pull down

GST-fusion proteins were incubated with GSH agarose (Pierce) for GST pull down in PBS buffer for 1 h at 4 °C. After the GSH agarose was washed with PBS, His-tagged proteins were added and incubated with the cleaned agarose for 1 h at 4

°C in PBS buffer. After washing, the agarose-bound proteins were analyzed by Western blot.

Bimolecular fluorescence complementation assay

The gene sequences of $G6PD^{WT}$, $G6PD^{R198P}$, $G6PD^{H263A}$, AMPKα1, NAMPT, and NADK1 were cloned into pCDH-(P_A-Vn)-P2A-mCherry-P2A-(P_B-Vc) expression vectors. 293T cells were transfected with these plasmids on the Confocal Dishes (NEST). At 24 h post-transfection, fluorescence images were collected with a confocal microscope system (Zeiss LSM880 Airyscan). The fluorescence intensity was quantified by ImageJ (1.53K).

G6PD enzymatic activity assay

G6PD enzymatic activity was determined by a G6PD activity assay kit (S0189, Beyotime Biotech Inc) according to the manufacturer's instructions. G6P, in the presence of $NADP^+$, is oxidized by G6PD to generate 6-phosphogluconolactone and NADPH. In the presence of an electron-coupled reagent 1-MPMS (1-methoxy-5-methylphenazinium Methyl Sulfate), NADPH reduces WST-8 to yellow Formazan with a maximum absorption peak at about 450 nm. The activity of Formazan in the reaction system is proportional to G6PD activity in this assay. Enzymatic activities of purified protein were normalized on the basis of total protein, which was determined with bicinchoninic acid assay kit. Enzymatic activities of cell lysates were normalized on the basis of G6PD expression in immunoblotting.

NAMPT enzymatic activity

NAMPT enzymatic activity was determined by a NAMPT Activity Assay Kit (catalog no.: #ab221819, Abcam) following the manufacturer's protocols. The assay is based on a multi-step reaction that converts WST-1 to WST-1 formazan, which can be easily detected at absorbance 450 nm. As the reaction is not stopped, we monitor the absorbance increase of WST-1 formazan at absorbance 450 nm every 2 min after the reaction is initiated to determine the velocity of the reaction. Initial velocity was determined by the slope of the initial linear portion of the enzyme kinetic curve.

NADK1 enzymatic activity

As for the effects of NADH on NADK1, the enzymatic activity was determined by ADP-Glo Kinase Assay (catalog no.: #V9104, Promega) according to the manufacturer's instruction. This is a homogeneous, signal increase assay that measures ADP production from a kinase reaction by coupled enzymes that first convert ADP to ATP and subsequently quantifies newly synthesized ATP using luciferase in the presence of luciferin. Since the unused ATP in the first step is depleted prior to ADP to ATP conversion, this assay shows excellent sensitivity over a wide range of ATP concentrations. In order to detect the effect of G6PD on NADK activity, NADP/NADPH-Glo assay kit catalog no.: #G9082, Promega) was used to test the production of $NADP^+$ and NADPH in the reaction system. Luciferin is detected using Ultra-Glo rLuciferase, and the amount of light produced is proportional to the amount of NADP+ and NADPH in a sample.

GAPDH activity assay

GAPDH enzymatic activity was determined by GAPDH Activity Assay Kit (ab204732, Abcam) following the manufacturer's instructions. GAPDH catalyzes the conversion of glyceraldehyde-3-phosphate (GAP) to 1, 3-bisphosphate glycerate (BPG) and the intermediate, NADH, which reacts with a developer to form a colored product that absorbs maximally at 450 nm. The activity of GAPDH can be reflected by measuring NADH production at 450 nm.

In vitro *kinase assays*

Flag-AMPKα1 was immunoprecipitated from HeLa/G6PD-KO cells that transfected with Flag-AMPKα1 plasmids. G6PD was purified from *E. coli* BL21. Kinase assay was carried out in the buffer (50 mM potassium acetate, 20 mM Tris-acetate, 10 mM magnesium acetate, 100 μg/ml bovine serum albumin) for 30 min at RT, using 200 ng AMPKα1 immunoprecipitate and 150 ng or 300 ng G6PD as substrates per reaction, in the presence or absence of 1 mM ATP.

Glucose uptake and lactate excretion in cells

Measurement of lactate and glucose concentrations in cell culture medium was performed using the M-100 Automatic Biosensors Analyzer (Shenzhen SiemenTechnology Co, Ltd) according to user instructions. Cell preparations and detection procedures were described as before (12). Briefly, cells were grown in 12-well plates at 2×10^5 cells per well and then were incubated with the treatment medium containing 10% dialyzed FBS, 10 mM glucose, 1 mM glutamine, and no pyruvate for 8 h. Cell media were collected at 0 h and 8 h. Aliquots of 100 μl medium were used to measure the concentration of glucose and lactate. The increased or reduced amount of metabolite in the medium, normalized for area under the curve, was the excretion or uptake of metabolite by cells per hour. The values were either directly presented or normalized for comparison with the control.

Glycerol excretion

Measurement of glycerol levels in cell culture medium was performed with a liquid sample glycerol assay kit (E1002, Applygen Technologies Inc) following the manufacturer's protocols. Glycerol is phosphorylated to glycerol 3-phosphate by glycerol kinase in the presence of ATP. Glycerol 3-phosphate is then oxidized by glycerol phosphate oxidase to produce hydrogen peroxide. In the peroxidase, the lower chromogenic substrate is converted to benzoquinone imine and its optical density is positive to glycerol concentration. The absorbance was measured at 550 nm.

GSH and GSSG assay

The intracellular GSH and GSSG levels were determined with GSH and GSSG assay kit (S0053, Beyotime Biotech Inc).

Cellular pellets (10 μl) were mixed with 30 μl of 5% metaphosphoric acid, then frozen and thawed twice using liquid nitrogen and 37 °C water. The samples were centrifuged, and the supernatant was subjected to GSH and GSSG assay. The total GSH level was measured by the 5,5-dithiobis (2-nitrobenzoic acid)-GSSG recycling assay. The absorbance was measured at 412 nm. The amount of total GSH in samples was calculated according to the standard curve. The amount of GSH was obtained by subtracting the amount of GSSG from the total GSH.

Metabolites isotope tracing

LC-MS/MS analyses were conducted on a TSQ Quantiva triple quadrupole mass spectrometer networked to a Dionex UltiMate 3000 UPLC system (Thermo Fisher Scientific) at the Metabolomics Facility at Tsinghua University Branch of China National Center for Protein Sciences (Beijing, China). Multiple reaction monitoring mode was developed using chemical standards. Experiments were performed in a medium containing 10% dialyzed FBS. DMEM lacking glucose, glutamine, pyruvate, and phenol red was prepared from powder (catalog no.: #DMP52 from Casson Labs) by adding 3.7 g $NaHCO_3$ per liter and adjusting the pH to 7.4 and then supplemented with 25 mM unlabeled glucose and 1 mM $^{13}C_5$-glutamine or 10 mM [3-^{2}H]-glucose and 1 mM unlabeled glutamine. For nicotinamide labeling, 32.8 μM [2,4,5,6-^{2}H]-nicotinamide was added to the phenol red–free RIPM1640 (BioInd), which intrinsically contains 11.1 mM glucose, 2.05 mM glutamine, and 8.2 μM label-free nicotinamide. As for polar metabolite analysis, cells were grown in 60 mm dishes (100 mm dishes for NADPH isotope tracing) until 80% confluent, then rinsed with PBS, and cultured with 6.5 ml ^{2}H-containing medium for 8 h under the normal condition for NADPH isotope tracing. Cells were extracted by freeze thawing three times in 0.5 ml 80% methanol (prechilled to −80 °C and 1 ml for 100 mm dishes) after they were rinsed twice with RT PBS. Macromolecules and debris were removed by centrifugation at 14,000*g* for 20 min at 4 °C, and the metabolite-containing supernatants were dried under nitrogen gas. Dried samples were stored at −80 °C and then resuspended in 50 μl water and prepared for LC-MS/MS analyses. One microliter of each sample was injected onto a Synergi Hydro-RP 100A 2.1 × 100 mm column (Phenomenex) for metabolite separation with column temperature at 35 °C. Mobile phases A and B were 10 mM thiobarbituric acid in aqueous with pH 5.0 and 100% methanol, respectively. The chromatographic gradient was set for mobile phase B as follows: 0 to 3.5 min, 1% B; 3.5 to 22 min, from 1% to 70% B; 22 to 23 min, from 70% to 90% B; 23 to 25 min, 90% B; 25 to 30 min, 1% B. Data were acquired using a positive/negative switching method. Spray voltages of 3.5 kV and 2.5 kV were applied for positive and negative modes, respectively. Q1 and Q3 resolution were set at 0.7, and 1 s of cycle time was used in the method. The abundance of each mass isotopomer was then mathematically corrected to eliminate natural abundance isotopes and finally converted into a percentage of the total pool.

Determination of cellular metabolites

HeLa/WT, HeLa^{KO}, HeLa^{WT}, HeLa^{R198P}, and HeLa^{H263A} cells were grown in 100 mm dishes until 80% confluent, then rinsed with PBS, and cultured with 8 ml phenol red–free DMEM that containing 10% dialyzed FBS, 25 mM glucose, and 1 mM glutamine for 24 h. Then samples were prepared as described in the section "Metabolites isotope tracing." Dried samples were stored at −80 °C and then resuspended in 50 μl 80% methanol and prepared for LC/MS analyses as described in the section "Metabolites isotope tracing."

Isotope tracing of fatty acids

Fatty acids analysis was performed on Q Exactive orbitrap mass spectrometer (Thermo) at the Metabolomics Facility at Tsinghua University Branch of China National Center for Protein Sciences (Beijing, China). HeLa cells were grown in 60 mm dishes with the initial seeding density of 6 × 10^5 cells and then were incubated normally for 48 h in the defined-medium based on DMEM, which contains 10% FBS dialyzed, 50 IU penicillin/streptomycin, 20 mM glucose, and 2 mM [U-^{13}C]-glutamine. Samples were prepared as previously described (29). Media were aspirated, and cells were rinsed twice with 2 ml RT PBS and then extracted with 1 ml 50% methanol solution containing 0.1 M HCl (prechilled to −80 °C). The resulting liquid and cell debris were scraped into a glass vial. Chloroform (0.5 ml) was added, the mixture was vortexed for 1 min and then centrifuged at 3000 rpm for 15 min, and the chloroform layer was transferred to a glass vial. The extract was dried under N_2, reconstituted into 1 ml 90% methanol solution containing 0.3 M KOH, incubated at 80 °C for 1 h to saponify fatty acids, acidified with 0.1 ml of formic acid, extracted twice with 1 ml of hexane, and dried under N_2. Dried samples were stored at −80 °C and then resuspended in 150 μl dichloromethane: methanol and prepared for LC/MS analyses (30). CORTECS C18 column (2.1 × 100 mm; Waters) was applied for analysis. Mobile phase A was prepared by dissolving 0.77 g of ammonium acetate in 400 ml of HPLC-grade water, followed by adding 600 ml of HPLC-grade acetonitrile. Mobile phase B was prepared by mixing 100 ml of acetonitrile with 900 ml of isopropanol. The gradient was as follows: 0 min, 37% B; 1.5 min, 37% B; 4 min, 45% B; 5 min, 52% B; 8 min, 58% B; 11 min, 66% B; 14 min, 70% B; 18 min, 75% B; 20 min, 98% B; 22 min, 98% B; 22.1 min, 37% B; 25 min, 37% B. Some MS parameters were different from polar compound analysis as follows: spray voltage, 3.2 kV for positive and 2.8 kV for negative; capillary temperature, 320 °C; aux gas flow rate (arb), 10; and mass range (m/z), 240 to 2000 for positive and 200 to 2000 for negative. Multiple reaction monitoring data were analyzed using Tracefinder. Lipids were assigned by a home-built lipid database in "screening" mode and quantified in "Quan" mode. Lipids were identified based on matching precursor and characteristic fragment masses. The 5 ppm and 10 ppm mass tolerance was used for precursor and fragment, respectively. Only the lipids with chromatographic area >5E6 were considered as confident identification. A 0.25 min

retention time shift was allowed for quantitation. Retention times and mass fragmentation signatures of all metabolites were validated using pure standards. Ion pairs with various ^{13}C labels were derived based on chemical structures of precursors and fragments. The abundance of each mass isotopomer was then mathematically corrected to eliminate natural abundance isotopes and finally converted into a percentage of the total pool. The percentage of labeled fatty acid carbons of the total pool (P) was calculated as the following (13):

$$P = \sum_{n=1,2,3...m}^{m} \frac{n}{m} * P_n$$

where n is the number of labeled carbons in an m-carbon fatty acid or cholesterol and P_n is the percentage of n-carbon–labeled fatty acid of the total pool. The areas of the ion peaks of interest were corrected by cell number. Finally, the relative abundance of metabolites was compared with each other.

In vivo *tumor growth*

Female nude mice between the ages of 4 to 6 weeks old were used for the tumor xenograft experiment. $G6PD^{KO}$, $G6PD^{WT}$, $G6PD^{R198P}$, and $G6PD^{H263A}$ tumor cells were injected subcutaneously at the right dorsal flank of recipient mice (5×10^6 cells per mouse, seven mice per group). The mice were observed for 6 weeks to monitor tumor growth and then sacrificed 6 weeks postinoculation. The weights of the tumors were measured after the mice were euthanized. All animal procedures were approved by the Animal Care and Use Committee of Capital Medical University.

Statistical analysis

Data are given as means ± SD. Statistical analyses were performed using unpaired two-tailed Student's *t* test for comparison between two groups. Asterisks in the figures indicated statistical significances ($^*p < 0.05$; $^{**}p < 0.01$).

Data availability

All data are included in the article.

Supporting information—This article contains supporting information.

Acknowledgments—We thank Dr Xiaohui Liu (Metabolomics Facility at Tsinghua University Branch of China National Center for Protein Sciences, China) for technical help. This work was supported by Grants 81972567 and 82030093 from the Natural Science Foundation of China, and Support Project for High-Level Teachers in Beijing Municipal Universities during the Period of 13th Five-Year Plan grant CIT&TCD20190333.

Author contributions—B. L. and J. N. conceptualization; B. L. and J. N. methodology; X. J., J. N., and B. L. formal analysis; X. J., L. L., B. Z, Y. H., and X. L. investigation; B. L. writing–original draft; B. L., J. N., and X. J. writing–review & editing.

Conflict of interest—The authors declare that they have no conflicts of interest with the contents of this article.

Abbreviations—The abbreviations used are: AICAR, 5-amino-4-imidazolecarboxamide ribonucleoside; Co-IP, coimmunoprecipitation; ETC, electron transport chain; FBS, fetal bovine serum; G6P, glucose-6-phosphate; G6PD, G6P dehydrogenase; IP, immunoprecipitation; MS, mass spectrometry; NAMPT, nicotinamide phosphoribosyltransferase; non-oxPPP, nonoxidative PPP; oxPPP, oxidative PPP; PMS, phenazine methosulfate; PPP, pentose phosphate pathway.

References

1. Stincone, A., Prigione, A., Cramer, T., Wamelink, M. M., Campbell, K., Cheung, E., *et al.* (2015) The return of metabolism: biochemistry and physiology of the pentose phosphate pathway. *Biol. Rev. Camb. Philos. Soc.* **90**, 927–963
2. Patra, K. C., and Hay, N. (2014) The pentose phosphate pathway and cancer. *Trends Biochem. Sci.* **39**, 347–354
3. Jiang, P., Du, W., and Wu, M. (2014) Regulation of the pentose phosphate pathway in cancer. *Protein Cell* **5**, 592–602
4. Chen, L., Zhang, Z., Hoshino, A., Zheng, H. D., Morley, M., Arany, Z., *et al.* (2019) NADPH production by the oxidative pentose-phosphate pathway supports folate metabolism. *Nat. Metab.* **1**, 404–415
5. Cappellini, M. D., and Fiorelli, G. (2008) Glucose-6-phosphate dehydrogenase deficiency. *Lancet* **371**, 64–74
6. Luzzatto, L., Nannelli, C., and Notaro, R. (2016) Glucose-6-phosphate dehydrogenase deficiency. *Hematol. Oncol. Clin. North Am.* **30**, 373–393
7. WHO, W. G. (1989) Glucose-6-phosphate dehydrogenase deficiency. *Bull. World Health Organ.* **67**, 601–611
8. Minucci, A., Moradkhani, K., Hwang, M. J., Zuppi, C., Giardina, B., and Capoluongo, E. (2012) Glucose-6-phosphate dehydrogenase (G6PD) mutations database: review of the "old" and update of the new mutations. *Blood Cell Mol. Dis.* **48**, 154–165
9. Dubreuil, M. M., Morgens, D. W., Okumoto, K., Honsho, M., Contrepois, K., Lee-McMullen, B., *et al.* (2020) Systematic identification of regulators of oxidative stress reveals non-canonical roles for peroxisomal import and the pentose phosphate pathway. *Cell Rep.* **30**, 1417–1433.e7
10. Longo, L., Vanegas, O. C., Patel, M., Rosti, V., Li, H., Waka, J., *et al.* (2002) Maternally transmitted severe glucose 6-phosphate dehydrogenase deficiency is an embryonic lethal. *EMBO J.* **21**, 4229–4239
11. Pandolfi, P. P., Sonati, F., Rivi, R., Mason, P., Grosveld, F., and Luzzatto, L. (1995) Targeted disruption of the housekeeping gene encoding glucose 6-phosphate dehydrogenase (G6PD): g6PD is dispensable for pentose synthesis but essential for defense against oxidative stress. *EMBO J.* **14**, 5209–5215
12. Liu, M., Wang, Y., Yang, C., Ruan, Y., Bai, C., Chu, Q., *et al.* (2020) Inhibiting both proline biosynthesis and lipogenesis synergistically suppresses tumor growth. *J. Exp. Med.* **217**, e20191226
13. Wang, Y., Bai, C., Ruan, Y., Liu, M., Chu, Q., Qiu, L., *et al.* (2019) Coordinative metabolism of glutamine carbon and nitrogen in proliferating cancer cells under hypoxia. *Nat. Commun.* **10**, 201
14. Zhong, B., Jiang, D., Hong, Y., Li, L., Qiu, L., Yang, R., *et al.* (2021) Glucose-6-phosphate dehydrogenase neutralizes stresses by supporting reductive glutamine metabolism and AMPK activation. *Signal Transduct. Target. Ther.* **6**, 46
15. Sanjana, N. E., Shalem, O., and Zhang, F. (2014) Improved vectors and genome-wide libraries for CRISPR screening. *Nat. Methods* **11**, 783–784
16. Cosgrove, M. S., Naylor, C., Paludan, S., Adams, M. J., and Levy, H. R. (1998) On the mechanism of the reaction catalyzed by glucose 6-phosphate dehydrogenase. *Biochemistry* **37**, 2759–2767
17. Kotaka, M., Gover, S., Vandeputte-Rutten, L., Au, S. W., Lam, V. M., and Adams, M. J. (2005) Structural studies of glucose-6-phosphate and NADP+ binding to human glucose-6-phosphate dehydrogenase. *Acta Crystallogr. D Biol. Crystallogr.* **61**, 495–504

18. Lewis, C. A., Parker, S. J., Fiske, B. P., McCloskey, D., Gui, D. Y., Green, C. R., *et al.* (2014) Tracing compartmentalized NADPH metabolism in the cytosol and mitochondria of mammalian cells. *Mol. Cell* **55**, 253–263
19. Chan, E., and Weiss, B. (1987) Endonuclease IV of escherichia coli is induced by paraquat. *Proc. Natl. Acad. Sci. U. S. A.* **84**, 3189–3193
20. Fearnhead, H. O., Dinsdale, D., and Cohen, G. M. (1995) An interleukin-1 beta-converting enzyme-like protease is a common mediator of apoptosis in thymocytes. *FEBS Lett.* **375**, 283–288
21. Wang, K., Li, J., Degterev, A., Hsu, E., Yuan, J., and Yuan, C. (2007) Structure-activity relationship analysis of a novel necroptosis inhibitor, necrostatin-5. *Bioorg. Med. Chem. Lett.* **17**, 1455–1465
22. Bogacz, M., and Krauth-Siegel, R. L. (2018) Tryparedoxin peroxidase-deficiency commits trypanosomes to ferroptosis-type cell death. *Elife* **7**, e37503
23. Gao, X., Zhao, L., Liu, S., Li, Y., Xia, S., Chen, D., *et al.* (2019) gamma-6-Phosphogluconolactone, a byproduct of the oxidative pentose phosphate pathway, contributes to AMPK activation through inhibition of PP2A. *Mol. Cell* **76**, 857–871.e9
24. Sullivan, J. E., Brocklehurst, K. J., Marley, A. E., Carey, F., Carling, D., and Beri, R. K. (1994) Inhibition of lipolysis and lipogenesis in isolated rat adipocytes with AICAR, a cell-permeable activator of AMP-activated protein kinase. *FEBS Lett.* **353**, 33–36
25. Kim, J., Yang, G., Kim, Y., Kim, J., and Ha, J. (2016) AMPK activators: mechanisms of action and physiological activities. *Exp. Mol. Med.* **48**, e224
26. Liu, L., Su, X., Quinn, W. J., 3rd, Hui, S., Krukenberg, K., Frederick, D. W., *et al.* (2018) Quantitative analysis of NAD synthesis-breakdown fluxes. *Cell Metab.* **27**, 1067–1080.e5
27. Zhang, Y., Xu, Y., Lu, W., Ghergurovich, J. M., Guo, L., Blair, I. A., *et al.* (2021) Upregulation of antioxidant capacity and nucleotide precursor availability suffices for oncogenic transformation. *Cell Metab.* **33**, 94–109.e8
28. Li, B., Gordon, G. M., Du, C. H., Xu, J., and Du, W. (2010) Specific killing of Rb mutant cancer cells by inactivating TSC2. *Cancer Cell* **17**, 469–480
29. Kamphorst, J. J., Cross, J. R., Fan, J., de Stanchina, E., Mathew, R., White, E. P., *et al.* (2013) Hypoxic and Ras-transformed cells support growth by scavenging unsaturated fatty acids from lysophospholipids. *Proc. Natl. Acad. Sci. U. S. A.* **110**, 8882–8887
30. Xu, L., Wang, X., Jiao, Y., and Liu, X. (2018) Assessment of potential false positives via orbitrap-based untargeted lipidomics from rat tissues. *Talanta* **178**, 287–293